Study of low peak power highly coherent broadband supercontinuum generation through dispersion engineered Si-rich Silicon Nitride Waveguide

M. R. Karim[1,*], **Nayem Al Kayed**[2], **Md Rabiul Hossain**[3], **and B. M. A. Rahman**[4]

[1] *Department of Electrical and Electronic Engineering, Chittagong Independent University, Chittagong, Bangladesh*
[2] *Department of Electrical and Electronic Engineering, Chittagong University of Engineering and Technology, Chittagong, Bangladesh*
[3] *Department of Electronics and Telecommunication Engineering, Chittagong Independent University, Chittagong, Bangladesh*
[4] *Department of Electrical and Electronic Engineering, City University of London, London, UK*
[*] *Corresponding author: mrkarim@ciu.edu.bd*

Compiled May 30, 2020

Since the first observation by Alfano and Shapiro in the 1970s, supercontinuum generation study has become an attractive research area in the field of broadband light source design for utilizing it in various applications associated with nonlinear optics in recent years. In this work, the numerical demonstration of ultrabroadband supercontinuum generation in the mid-infrared region by using complementary metal-oxide-semiconductor compatible Si-rich Silicon Nitride as core in a planar waveguide design employing two different cladding materials either of $LiNbO_3$ or MgF_2 glass as top and bottom, are explored. A rigorous numerical investigation of broadband source design in the mid-infrared using 2 mm long Si-rich Silicon Nitride Waveguides are studied in depth in terms of waveguide structural parameter variations, input peak power variation, unexpected deformation variation of the waveguide along the core region during fabrication, and spectral coherence analysis. Among the several waveguide models studied, two promising designs are identified for wideband supercontinuum generation up to the mid-infrared using very low input peak power of 50 W. Simulation results from the output of one of the proposed models reveal that the spectral coverage spanning from 0.8 μm to 4.6 μm can be obtained by the $LiNbO_3$ cladded waveguide and nearly a similar spectral coverage can be predicted by the other design, MgF_2 cladded waveguide. To the best of our knowledge, this can be the widest spectra spanning in the MIR region employing Si-rich Silicon Nitride Waveguide so far. In dispersion tuning as well as in supercontinuum generation, the effect of the occurrence of possible unexpected waveguide deformation around the core region during fabrication is studied. No significant amount of spectral changes of the proposed model for a maximum of 10 degrees inside/outside variation along the width are observed. However, even 1 degree up/down variation along the thickness could occur substantial spectral change at the waveguide output. Finally, the obtained output spectra from the proposed waveguides are found highly coherent and can be applied in various mid-infrared region applications such as optical coherence tomography, spectroscopic measurement, and frequency metrology.

OCIS codes: (320.6629) Supercontinuum generation; (260.3060) Infrared; (260.2030) Dispersion; (230.7390) Waveguides, planar;(030.1640) Coherence; (320.7110) Ultrafast nonlinear optics; (250.4390) Nonlinear optics, integrated optics; (220.0220) Optical design and fabrication.

http://dx.doi.org/10.1364/ao.XX.XXXXXX

INTRODUCTION

Nonlinear optics has become an alluring field of research in recent years due to the immense advancement in ultrafast optics technology [1]. In this arena, supercontinuum generation (SCG) is a particular branch of study to investigate ultrafast broadband spectra which can evolve through the nonlinear interaction of light inside the pulse propagation medium [2]. The state-of-the-art fabrication process makes it possible to extend the SCG coverage to the mid-infrared (MIR) which facilitates so many applications in telecommunication and biomedical sectors [3], [4]. Lately, the SCG in the MIR region found itself applicable in some impressive applications such as atomic spectroscopy [5], frequency metrology [6] etc.

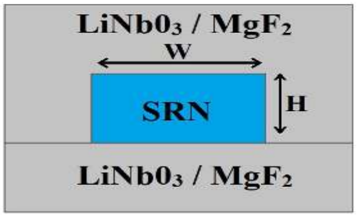

Fig. 1. Proposed waveguide geometry

To construct the ultrawideband SCG spectrum, Silica (SiO_2) based complementary metal-oxide-semiconductor (CMOS) compatible Silicon-On-Insulator (SOI) platform is extensively used [7]. Significant advancement in CMOS compatible technology has facilitated the SOI platform for the various scale of integrated Silicon photonics device fabrication. The SOI platform is capable of building scalable chip integrated components by assuring their linear or nonlinear properties [8–12]. Among several nonlinear materials used on-chip integrated photonics platform for the broadband SCG generation, the Si-rich Silicon Nitride (SRN) material with Si:N ratio of 2:1 is a promising candidate in this on-chip platform to generate the broad bandwidth SCG up to the MIR due to its large Kerr nonlinear parameter (n_2 = 2.8 $\times$ 10^{-13} cm^2/W), high linear refractive index (n = 3.1) and an extended energy band gap (2.05 eV) at 1.55 μm wavelength [13]. Moreover, high shot to shot coherence over the entire SCG coverage can also be obtained owing to its low Raman response [14]. During chemical vapor deposition of the SRN material, the Si-H bonds are introduced which are the prime cause of material loss of this material [15].

In recent years, several research groups have performed broadband SCG investigation from the deep ultraviolet to the MIR theoretically and experimentally by using the various planar structures made of Si_3N_4 and SRN materials [14, 16–23]. Spectrum spanning from 0.488 μm to 0.978 μm in a 10 mm long Si_3N_4 planar waveguide, which is made of SiO_2 as a lower cladding and air as an upper cladding, has been observed by Zaho *et al* [16] using Ti: Sapphire laser pumped at 0.795 μm wavelength with a duration of 100 fs at a pulse peak power of 874 W. Experimental demonstration of Salem *et al* [17] obtains the spectral coverage from 1.25 μm to 2.6 μm in 20 mm long stoichiometric Si_3N_4 waveguide by using all-fiber femtosecond laser pumped at 1.92 μm wavelength with 92 fs duration and 2000 W peak power. In the same year, using 8 mm long Si_3N_4 planar waveguide, spectral broadening from 0.673 μm to 1.944 μm is observed while pumping at 1.03 μm as pump wavelength with 92 fs duration at a peak power of 4750 W [14]. By using 50 W as pump peak power and employing 2.6 μm as pump wavelength in Si_3N_4 micro-resonator, Luke *et al* [18] noticed a spectral spreading from 2.3 μm to 3.5 μm. From 0.470 μm to 2.130 μm broadened SCG in CMOS compatible Si_3N_4 waveguide is achieved by Epping *et al* [19] having pump wavelength of 1.064 μm with 115 fs pulse duration at a peak power of 5100 W. Flat spectra from 0.526 μm to 2.6 μm in stoichiometric Si_3N_4 waveguide using 1.56 μm as center wavelength with the duration of 120 fs at a peak power of 11700 W has been reported in [23]. In [20], Karim *et al* observed wide spectra broadening from 0.8 μm to 6.5 μm in 10 mm long stoichiometric Si_3N_4 planar waveguide numerically by choosing a pump source in 1.55 μm wavelength with 50 fs duration at a peak power of 5000 W. Spectral coverage from 1.130 μm to 1.750 μm in the SRN waveguide made of SiO_2 as cladding and pumping at 1.55 μm with 500 fs duration at a peak power of 140 W is reported in [21]. Using Er-Fiber laser, Liu *et al* [22] performed a detailed investigation and observed a spectral spanning from 0.820 μm to 2.250 μm through 10 mm long SRN waveguide while pumping at 1.555 μm as the center wavelength with 105 fs pulse duration at a peak power of 1330 W.

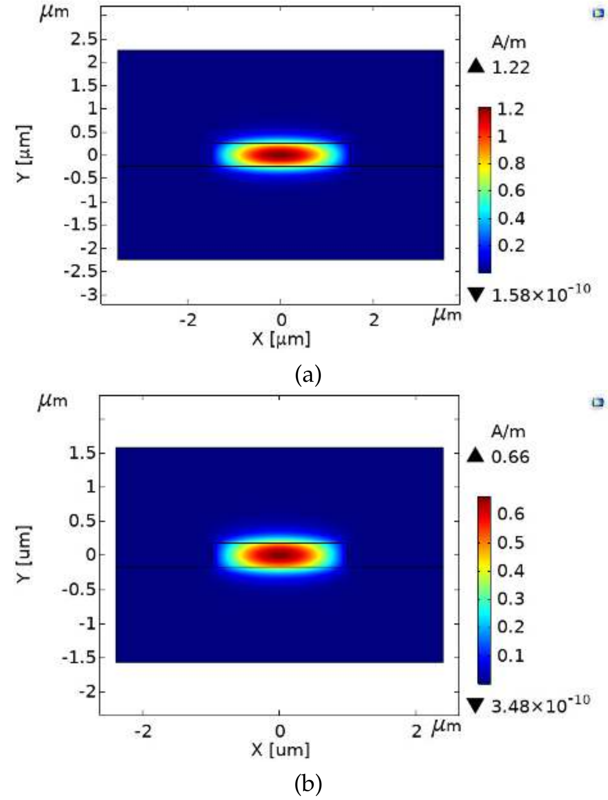

Fig. 2. Field profiles (transverse cross sectional view) of FQTE mode are obtained by the COMSOL for a rectangular waveguide at the 1.55 μm wavelength: (a) $W \times H$ = 3 μm $\times$ 0.5 μm for the $LiNbO_3$ cladded waveguide; (b) $W \times H$= 2 μm $\times$ 0.35 μm for the MgF_2 cladded waveguide.

Apart from using silicon nitride material, some other nonlinear materials such as tellurite, fluoride, and chalcogenide (ChG) [24] are used to design broadband SCG sources for various MIR region applications. The ChG glass system, among those, is the prominent one for broadband SCG generation in the MIR owing to the higher Kerr nonlinearity and the wider transmission limit ($\sim$ 25 μm). Among several broadband SCG sources made using ChG glass system reported until today, a few fiber structure SCG sources designed using optical step-index fiber based principle [25, 26] have attracted the research community a lot for achieving spectral coverage up to the far MIR. Yu *et al.* [25] has demonstrated a MIR SCG coverage extending from 1.8 to 10 μm with a pulse of 330-fs duration when pumped at 4 μm in an 11-cm-long ChG step-index fiber made from $Ge_{12}As_{24}Se_{64}$ glass system as a core and $Ge_{12}As_{24}S_{64}$ glass system as an outer cladding with an input peak power of 3 kW. Cheng *et al.* [26] has reported a MIR SCG expansion covering the wavelength range from 2 to 15.1 μm in a 3-cm-long ChG step-index fiber using As_2Se_3 glass as the core and $AsSe_2$ glass as an outer cladding when pumped at 9.8 μm with a pulse duration of 170-fs and a peak power of 2.89 MW.

Table 1. Sellmeier fitting co-efficients

Materials	Si_2N[13]		$LiNbO_3$ [27]		MgF_2[28]	
N	α_k	β_k	α_k	β_k	α_k	β_k
k=1	2.21715	0.0632602	2.67334	0.01764	0.48755108	0.04338408
k=2	1.12108	0.249134	1.2290	0.054914	0.39875031	0.09461442
k=3	24.8224	250.091	12.614	474.600	2.3120353	23.793604
k=4	17.6617	251.079	-	-	-	-

In this work, two 2 mm long CMOS compatible dispersion engineered SRN waveguides using two different claddings have been proposed separately for investigating the MIR SCG in the anomalous dispersion regime. One of the optimized waveguides is over and under cladded by the $LiNbO_3$ and the other one is by the MgF_2 glass. In case of the MgF_2 cladded waveguide, the spectral coverage from 0.8 μm to 4.7 μm is observed by employing the pump source at 1.55 μm wavelength with 50 fs pulse duration at a low peak power of 50 W. Similar pumping condition has been applied to the $LiNbO_3$ cladded waveguide by which a SCG spectrum can be predicted from 0.8 μm to beyond 4.6 μm. It is a matter of consideration that in most of the above mentioned works (in the literature review), the SiO_2 glass is used as cladding. Since the SiO_2 glass has high material absorption loss beyond 2.3 μm [29], as the MgF_2 and the $LiNbO_3$ have the transmission limit beyond 7 μm [28] and 5 μm [27], respectively, the SRN waveguides proposed here have been modeled for the wideband SCG coverage into the MIR by employing either of these cladding materials as top and bottom during the waveguide design. Although several works have been done by the researchers using the MgF_2 glass as cladding [30–36], however, to the best of the authors' knowledge, the proposed approach, waveguide design using the $LiNbO_3$ as top and bottom cladding, has not been studied yet. Moreover, the effects of an input power variation and the occurrence of deformation during waveguide fabrication on the output SCG bandwidth are studied in detail. Finally, the spectral coherence of the proposed models is tested and is obtained a highly coherent SCG outcome at the waveguide output.

MODELING AND METHODS

Graphical diagram of the proposed planar SRN waveguide either with $LiNbO_3$ or MgF_2 glass as top and bottom claddings is shown in Fig. 1. In this work, the linear refractive index of Si_2N is computed by the Sellmeier Eq. 1, $LiNbO_3$ and MgF_2 glass materials linear refractive indices are calculated by the Sellmeier Eq. 2. The corresponding Sellmeier fitting co-efficients are given in the Table 1.

$$n(\lambda) = 1 + \sqrt{1 + \sum_{k=1}^{N} \frac{\alpha_k \lambda^2}{\lambda^2 - \beta_k^2}} \quad (1)$$

$$n(\lambda) = \sqrt{1 + \sum_{k=1}^{N} \frac{\alpha_k \lambda^2}{\lambda^2 - \beta_k^2}} \quad (2)$$

where the value of λ is defined in μm.

Effective refractive index (n_{eff}) of the proposed waveguide up to the desired wavelength region considering the fundamental mode is calculated through finite element analysis (FEA) based COMSOL Multiphysics software. The electric field patterns of the fundamental quasi-TE mode (FQTE) for the proposed waveguides made of the $LiNbO_3$ cladded waveguide ($W \times H$ = 3 μm$\times$ 0.5 μm) and the MgF_2 cladded waveguide ($W \times H$ = 2 μm$\times$ 0.35 μm) have been depicted in the Figs. 2(a) and 2(b), respectively. The maximum value of the magnetic field of FQTE mode for both the proposed waveguides are obtained through COMSOL as 1.22 A/m and 0.66 A/m respectively at the 1.55 μm wavelength. The computational process of the key parameter, group velocity dispersion (GVD) for generating the efficacious SCG spectral coverage up to the desired wavelength, has been thoroughly discussed. To study and to visualize the evolution of the SCG at the proposed waveguides output, a detailed investigation is performed in the anomalous dispersion region by numerically solving the generalized nonlinear Schrödinger equation (GNLSE) for mono-polarized pulse propagation [37]:

$$\frac{\partial A}{\partial z} = -\frac{\alpha}{2}A + \sum_{k\geq 2}^{12} \frac{i^{k+1}}{k!}\beta_k \frac{\partial A^k}{\partial T^k} + i\gamma(|A|^2 A + \frac{i}{\omega_0}\frac{\partial}{\partial T}|A|^2 A) \quad (3)$$

In the GNLSE equation, A(z,T) denotes the pulse envelope which evolves throughout the wavelength of a waveguide i.e. a retarded time frame with reference $T = t - \beta_1 Z$ moving at the group velocity $v_g = \frac{1}{\beta_1}$. β_k (k$\geq$2) are the higher order Taylor series expanded dispersion coefficients around the center angular frequency ω_0 and the associated attenuation coefficient of SRN material is α. The nonlinear parameter is described as $\gamma = \frac{n_2 \omega_0}{c A_{\text{eff}}}$, where n_2 is the Kerr-nonlinearity at the pump wavelength and $A_{\text{eff}} = \frac{(\int\int |E^2| dxdy)^2}{(\int\int |E|^4 dxdy)}$ is the mode effective area for the fundamental mode. The Raman terms in the GNLSE have been neglected due to the insignificant Raman response of the SRN material [20].

NUMERICAL RESULTS AND ANALYSIS

To attain efficacious SCG for a wide spectrum range up to the MIR, the proposed waveguides have been engineered in such that numerical simulation can be carried out in the anomalous dispersion region. The linear computational analysis is performed for simulating the waveguides at 1.55 μm wavelength in the anomalous GVD region by varying W and H. Several geometries of the SRN waveguide have been optimized for achieving the zero-dispersion wavelength (ZDW) in the vicinity to the wavelength selected for the pump source to be used during numerical simulations. Generation of an efficient spectrum

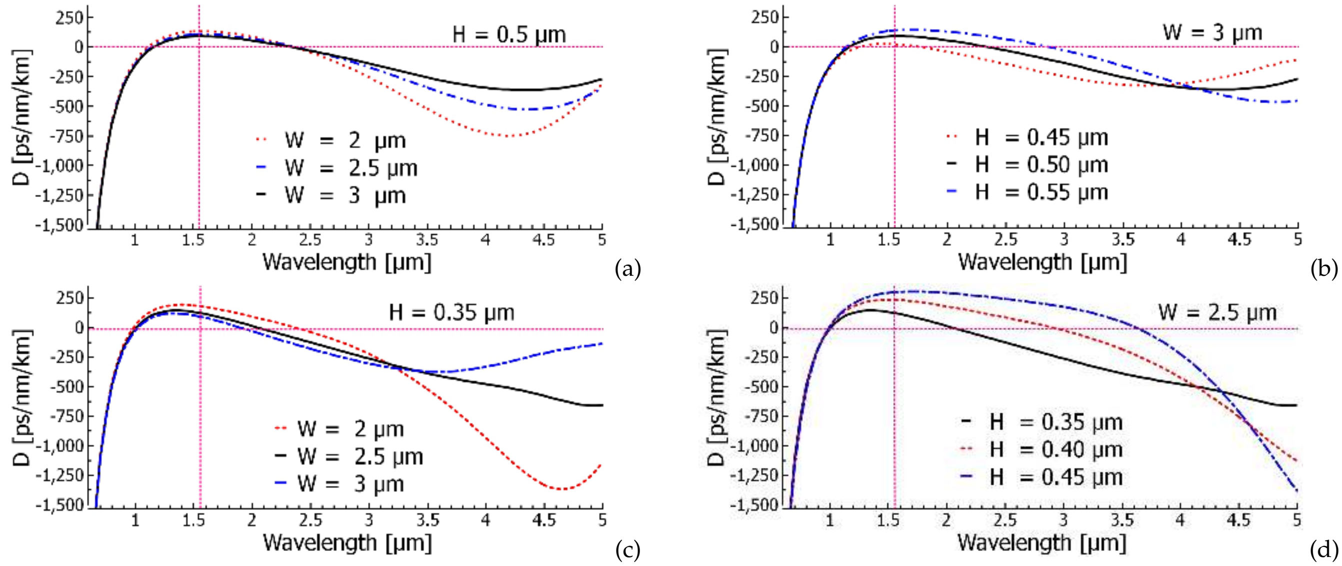

Fig. 3. Four sets of dispersion (GVD) curves depicted for the proposed SRN waveguide with two different cladding shown in Fig. 1 simulated at the selected pump source wavelength of 1.55 μm to obtain an (a) anomalous GVD region of the $LiNb0_3$ cladded waveguide by changing W from 2 μm to 3 μm with a step of 0.5 μm keeping H fixed at 0.5 μm; (b) anomalous GVD region of the $LiNb0_3$ cladded waveguide keeping structural width, W = 3 μm constant by varying thickness, H between 0.45 μm and 0.55 μm with a step of 50 nm; (c) anomalous GVD region of the MgF_2 cladded geometry by varying W from 2 μm to 3 μm with a step of 0.5 μm keeping H constant at 0.5 μm; (d) anomalous GVD region of the MgF_2 cladded geometry keeping waveguide W = 2.5 μm constant by changing H from 0.35 μm to 0.45 μm with a step of 50 nm; Vertical dotted lines indicate the pump wavelength.

reaching beyond the proposed SRN material transparency limit i.e. up to 5 μm is the prime aim of this work. Since the effective SCG expansion up to the wide wavelength region is dependent on the location of the pump wavelength selection, the desired SCG expansion can be obtained then if the location of the chosen pump source wavelength could able to be placed near the long wavelength side of the first ZDW of each design. This also induces a good impact on soliton order which make large frequency shifts due to a small anomalous dispersion GVD value obtained at the pump wavelength.

Figure 3 demonstrates the four-sets of GVD plots for the proposed waveguides of different geometries, which are optimized for pumping in the anomalous dispersion region. Initially, among several waveguide structures studied, the GVD (D) value of the $LiNbO_3$ cladded waveguide with dimensions H = 0.5 μm, W = 2 μm is found to be 131 ps/nm/km at the pump wavelength. While changing waveguide W from 2 μm to 3 μm with a step of 0.5 μm keeping H constant at 0.5 μm, the value of D at the pump wavelength approaches closer to the ZDW, which eventually reduces the D value of the corresponding design as shown in Fig. 3(a). In this case, the individual GVD curve shifts right with lowering GVD slope which results a minimum D = 89.4 ps/nm/km at our chosen pump wavelength for W = 3 μm waveguide among the three waveguide geometries proposed. Although D changes with W variation, however, the anomalous GVD region for this set of geometries remains the same. In Fig. 3(b), the GVD curves for different H are presented by keeping W fixed at 3 μm. When the value of H is being increased/decreased in steps of 50 nm, it is noticed that the GVD curve moves up or moves down significantly in the vertical direction which changes the D value at the pump wavelength substantially. Thus, the substantial changes of the anomalous GVD region can be obtained solely through H variation of the proposed waveguides. The GVD value at 1.55 μm is increased as the value of H increases. The above analysis indicates that the anomalous GVD region can not be regulated substantially by varying W of the waveguide, whereas an opposite behavior is observed while H is varied. Nevertheless, a little variation in

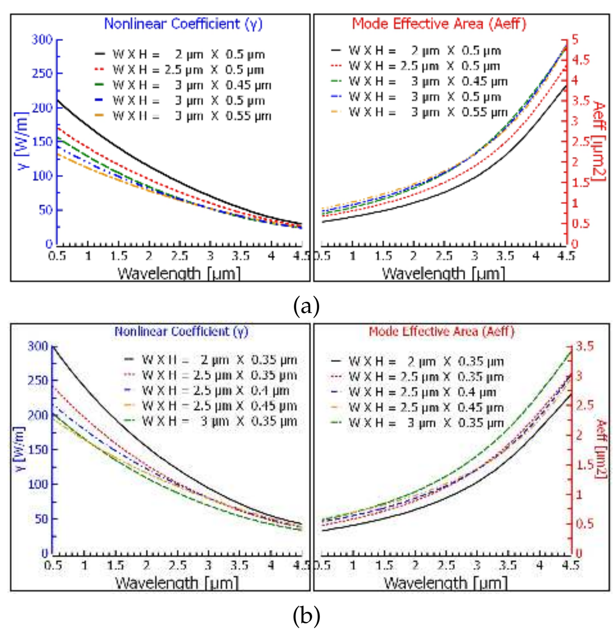

Fig. 4. Variation of mode effective areas and their corresponding nonlinear coefficients are calculated over the interested wavelength region for (a) the proposed $LiNbO_3$ cladded geometric structures (the values of H and W have given inside the figure); (b) the proposed MgF_2 cladded geometric structures (the values of H and W given inside the figure).

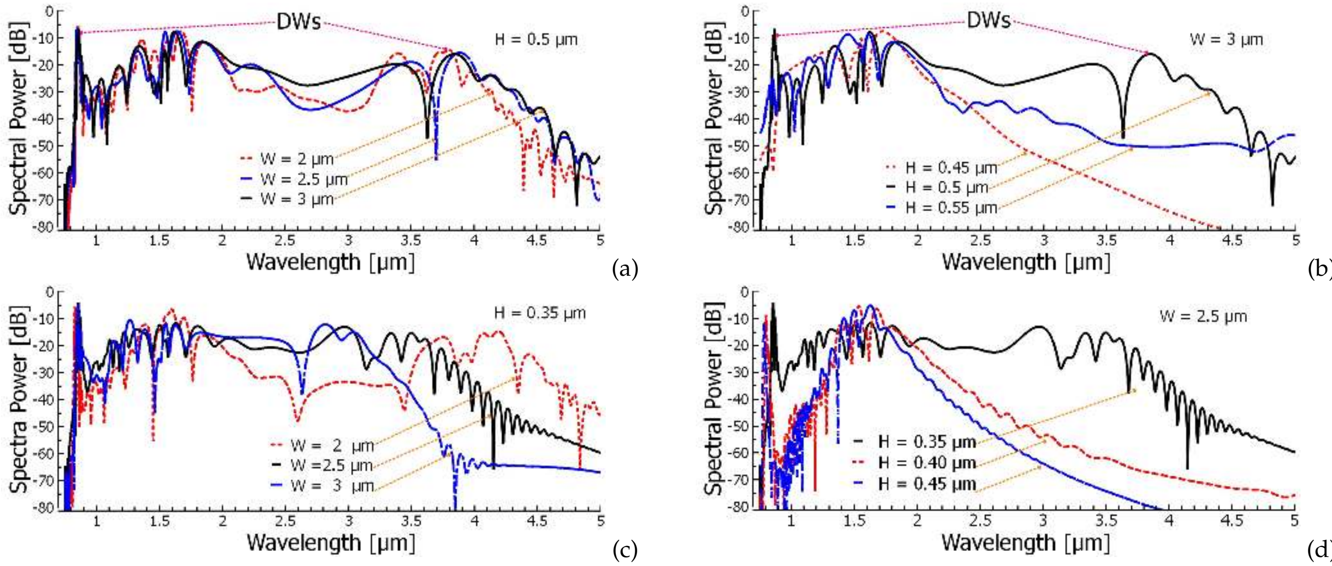

Fig. 5. Four sets of SCG spectra demonstrated in Fig. 3. depicted for a 2 mm long optimized SRN waveguide geometry with two different cladding (upper sets with the $LiNbO_3$ cladded and lower sets with the MgF_2 cladded) proposed in Fig. 1 by using a pump at 1.55 μm during simulation with a 50-fs sech pulse and an input peak power of 50 W.

H is required during waveguide modeling since the proposed model is highly sensitive in dispersion tuning rather than the variation of W. Figure 3(c) and Figure 3(d) presents a resemblant analysis for the MgF_2 cladded SRN waveguide to extract the dispersion curve. For the same H = 0.35 μm with different W, the GVD variations for three waveguide structures are shown in Fig. 3(c). In addition to that, keeping W = 2.5 μm, the waveguide structures of three different H are also investigated and are shown in Fig. 3(d). For the structure having W = 2 μm and H = 0.35 μm, the value of D obtained at 1.55 μm wavelength is 181 ps/nm/km. Further reducing H results a normal dispersion GVD curve. However, setting W = 3 μm keeping H same, the D value could be reduced to 92 ps/nm/km for the MgF_2 cladded SRN waveguide.

The numerical analysis for the SCG evolution in the MIR can be performed by solving the GLNSE given in [6]. The methodology of analysis adopted in this work follows [20] where it is cleared that, there is a probability of having a spurious solution during computation unless a sufficient amount of dispersion terms are used. So that, the GNLSE Eq. 3 is solved by employing the split-step Fourier method (SSFM) where higher-order dispersion terms up to 12th order are used. The number of grid points is as 2^{17}. To neglect the negative frequency evolution, the time step is as 2.76 fs. Along the propagation direction, the axial number of steps is chosen as 10^5 with a step size of 100 nm. The nonlinear parameter n_2 is 2.8×10^{13}cm^2/W and the estimated loss is 6 dB/cm at 1.55 μm for the SRN material [13] proposed. The pump is set at 1.55 μm wavelength and a transverse electric (TE) polarized full-wave at half-maximum (FWHM) sech pulse of 50 fs duration along with an input peak power of 50 W is launched during all numerical simulations. The length of the proposed waveguides is considered to be 2 mm long throughout the analysis. The responses as the SCG outcomes from different optimized geometries have been investigated thoroughly by varying several parameters during numerical simulations. The A_{eff} for those waveguide geometries are calculated using FEA based COMSOL solver and the corresponding nonlinear coefficients (γ) are calculated up to the desired wavelength. The variation of A_{eff} and the corresponding γ over the interested wavelength region are shown in Fig. 4. The estimated A_{eff} are 0.8214 μm^2, 0.9968 μm^2, 1.113 μm^2, 1.1724 μm^2 and 1.2351 μm^2 and the corresponding γ are 138.17 W/m, 113.86 W/m, 100.33 W/m, 96.81 W/m and 91.90 W/m respectively for the $LiNbO_3$ cladded waveguide at 1.55 μm wavelength for the dimensional parameter variation shown in Fig. 4(a). The corresponding values of D obtained for those structures are 130.78 ps/nm/km, 105.43 ps/nm/km, 21.06 ps/nm/km, 89.3967 ps/nm/km and 137.1135 ps/nm/km, respectively. A similar procedure is applied to obtain A_{eff} and γ which are shown in Fig. 4(b) for MgF_2 cladded waveguide and the estimated A_{eff} are 0.5979 μm^2, 0.7270 μm^2, 0.7729 μm^2, 0.8318 μm^2 and 0.8563 μm^2 and their corresponding γ are 189.84 W/m, 156.12 W/m, 146.85 W/m, 136.45 W/m and 132.55 W/m, respectively. Also, the values of D for those corresponding structures are estimated as 180.52 ps/nm/km, 123.35 ps/nm/km, 297.27 ps/nm/km, 232.88 ps/nm/km and 91.82 ps/nm/km, respectively.

It is obvious from Fig. 3(a) that the variation of W for the $LiNbO_3$ cladded waveguide hasn't changed the effective anomalous dispersion region significantly. As a result, the spectral broadening at the waveguide output remains similar for this set of waveguide models. The estimated SCG expansion for this set is covered the wavelength range 0.7–4.2 μm, 0.7–4.4 μm, and 0.7–4.5 μm that are corresponding to the spectra shown in Fig. 5(a). The Raman induced self-frequency shift (RIFS) has not occurred in this spectral evolution because of the low Raman response of the SRN material. The dynamics of evolving the SCG is quite similar to the mechanism described in [20]. Two dispersive waves (DWs) have been visualized for having two ZDWs on GVD curves: one is at 0.9 μm wavelength and the center of the other one is around 4 μm of the spectra. The response of the SCG for the different structural dimensions was obtained by tailoring the waveguide width from 2 μm to 3 μm fixing a thickness at 0.5 μm. In the 2nd set of modeling shown in Fig. 5(b), a narrowband spectrum is obtained in the range 0.9–2.5 μm for the geometry having H = 0.45 μm. However, increasing H at 0.5 μm results nearly a flattened SCG extended up to 4.5 μm. Further increasing H (at 0.55 μm) results a more longer wavelength extension with a dip in the middle of the spectra. Two DWs in the short and the long wavelengths are found as the previous design. However, the long-wavelength side DW is shifted to right (not shown in the plot as wavelength scale end at 5 μm) while H enhanced at 0.55 μm. Therefore, further increasing H results of an extended SCG with a dip i.e. power depletion between the pump wavelength and the long wavelength DW of the spectra. The output SCG of this set of structures indicates that the spectral spanning in the long-wavelength region for the individual model is dependent on the position of long-wavelength ZDW of the respective dispersion curve. Thus, the reduction of the anomalous GVD region limited the spectral broadening for the proposed design. The position of short-wavelength side DW for each design is located approximately at the same place for both sets of modeling described above. These phenomena can also be visualized from the spectral and temporal density graphs given in Fig. 6(a) and Fig. 6(b), respectively.

A similar procedure is adopted to study the SCG evolution in the MgF_2 cladded waveguide and to optimize a number of geometries of this model for further investigation as earlier. For W variation keeping H constant waveguide, the SCG expansion for the optimized structures (dimensional parameters described inside the figure) and the corresponding GVD curves are depicted in Fig. 5(c) and Fig. 3(c), respectively. The maximum spectral evolution can be obtained covering the wavelength range 0.8-4.7 μm for dimensional parameters W = 2 μm and H = 0.35 μm with a small dip between the short and the long wavelength side (nearly in the middle) of the spectrum. However, spectra are flattened out with increasing W which results narrowing the spectral bandwidth range for the next consecutive design. Afterward, the structural variation of H keeping W constant in the next set of MgF_2 cladded SRN waveguides are analyzed. Figs. 5(d) and 3(d) depict the obtained SCG for optimized geometries (dimensional parameters described inside the figure) and the corresponding set of GVD curves, respectively. Covering the wavelength range 0.8-4 μm with flattened output is obtained with dimensional parameters W = 2.5 μm and H = 0.35 μm, where this wavelength range is the maximum flattened spectral coverage predicted by the MgF_2 cladded waveguide proposed.

The spectral and temporal field profile for both the waveguides are demonstrated in Fig. 6. The dispersion length, $L_D = T_P^2/|\beta_2|$, the nonlinear length, $L_{NL} = 1/\gamma P$ are used to calculate the soliton order, $N = \sqrt{L_D/L_{NL}}$, which is later used to calculate the soliton fission length, $L_{\text{fiss}} = L_D/N$. The value of N and L_{fiss} for the proposed $LiNbO_3$ cladded waveguide are 5.85 and 1.2 mm, respectively as shown in the Figs. 6(a) and 6(b) where as from the Figs. 6(c) and 6(d), it is observed that those values are respectively 5.75 and 0.67 mm for the MgF_2 cladded waveguide. The spectral density at the 2 mm long output end for the proposed $LiNbO_3$ waveguide considering structural parameters W = 3 μm, H = 0.5 μm is shown in Fig. 6(a) and the corresponding spectra covering the wavelength region 0.8-4.6 μm has been depicted in Fig. 5(a) using a solid black line. The similar approach applies to investigate the SCG evolution of MgF_2 cladded waveguides and the spectral density plot for this design has been shown in Fig. 6(c) whose corresponding spectral coverage range 0.8-4.7 μm is denoted in Fig. 5(c) with a solid black line.

The effects of input power variations between 10 and 50 W are shown in Fig. 7 for both the waveguides proposed. For the $LiNbO_3$ cladded waveguide, Fig. 7(a) demonstrates the SCG coverage for waveguide structure of W = 3 μm, H = 0.5 μm. For a 10 W input power, the SCG covers the wavelength region 1.3-1.7 μm, whereas spectrum spanning from 0.7 to 2.4 μm is found while increasing the power from 10 to 20 W. Spectrum spanning is found beyond 4.6 μm as the power increased to 50

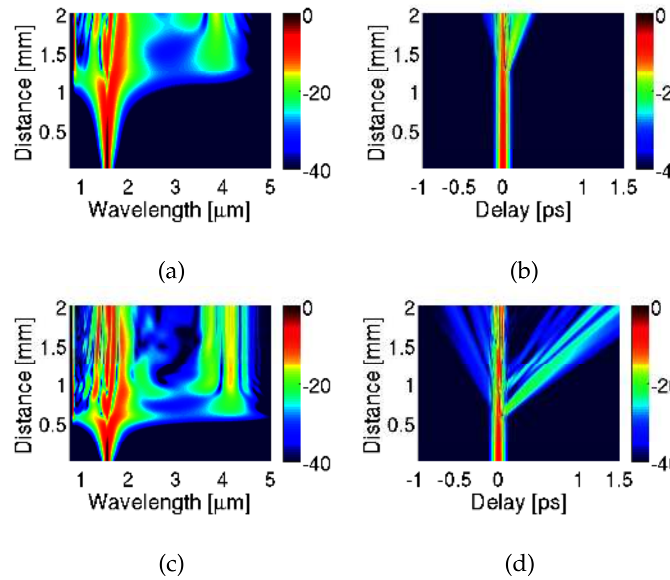

Fig. 6. The spectral density plot and the corresponding temporal density plot at the output of 2 mm long SRN waveguide where top row for the $LiNbO_3$ cladded geometry with dimensional parameters, H = 0.5 μm, W = 3 μm and lower row for the MgF_2 cladded geometry with dimensional parameters, H = 0.35 μm, W = 2 μm.

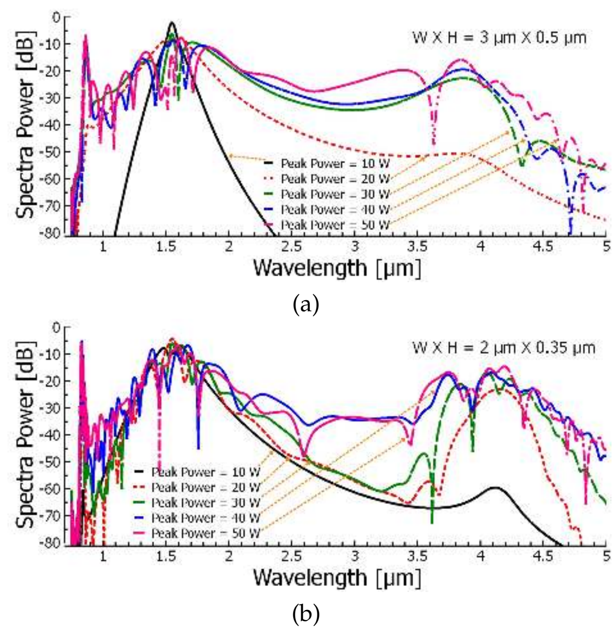

Fig. 7. Two sets of SCG spectra simulated by varying input peak power from 10 W to 50 W for (a) the $LiNbO_3$ cladded geometry with dimensional parameters, H = 0.5 μm, W = 3 μm; (b) the MgF_2 cladded geometry with dimensional parameters, H = 0.35 μm, W = 2 μm.

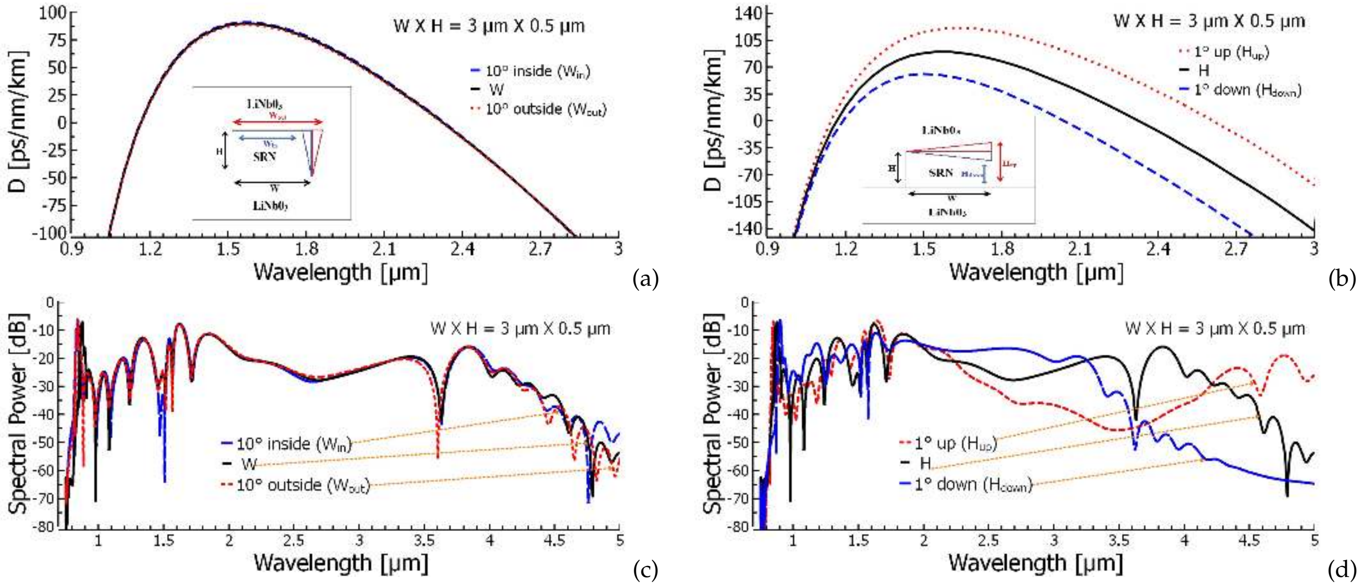

Fig. 8. The simulated GVD and the corresponding SCG coverage to observe the effects of deformation around the core of the $LiNbO_3$ cladded waveguide with (a) 10° inside (W_{in}) and 10° outside (W_{out}); (b) 1° up (H_{up}) and 1° down (H_{down}) and their corresponding SCG spectra are depicted in Figs. 8(c) and 8(d), respectively.

W. All spectral widths are approximated at -40 dB level from the peak. Further increment of input power flattened out the spectra rather than expansion for this design. Similarly, the spectral spanning, due to varying input peak power as shown in Fig. 7(b) in the MgF_2 cladded waveguide of dimension $W \times H$ = 2 μm $\times$ 0.35 μm, is investigated. Increasing input power, in this case, starts to flatten out the spectra, however, where dip still appears at the middle in the spectra as shown in Fig. 7(b). Long-wavelength side expansion, similar to the $LiNbO_3$ cladded model, does not occur as the further increment of peak power at the input for this design.

During fabrication, an unexpected deformation around the core region in either vertically or longitudinally or in both directions might have happened. The deformed geometric structures which are placed inside the GVD plots as shown in Fig. 8(a) and Fig. 8(b). Initially, the probable deformation is considered in W = 3 μm, H = 0.5 μm of the $LiNbO_3$ cladded waveguide. For 10° inside or 10° outside vertical side deformation as shown in the geometry given in an inset of Fig. 8(a), the optimized GVD curves considering the deformation amount mentioned and their corresponding SCG spectra are depicted in Fig. 8(a) and Fig. 8(c), respectively. After 10° inside deformation, the waveguide W is reduced to 2.91 μm and the estimated corresponding D value is 90.73 ps/nm/km. However, for 10° outside deformation, the waveguide W increases to 3.09 μm and the estimated D value becomes 88.46 ps/nm/km though the calculated D value is 89.4 ps/nm/km while considering an ideal case. From Figs. 8(a) and 8(c), it is obvious that for an inside or an outside deformation along the width up to 10° deformation, there are no significant changes observed either in the GVD plots or in the SCG spectra. On the other hand, the optimized GVD curves for 1° up/down deformation along the thickness are shown in Fig. 8(b). In case of a downward deformation, the waveguide H becomes 0.448 μm and the estimated D value is 60.02 ps/nm/km whereas for 1° up deformation, the waveguide H is 0.552 μm and the D value becomes 118.78 ps/nm/km. The corresponding SCG coverages are shown in Fig. 8(d) which implies a substantial SCG spectral variation at the waveguide output. For a downward deformation, 1000 nm bandwidth reduction occurs at the waveguide output, which is nearly 20 percent of the total expansion. In case of an upward deformation, the SCG expands with the expense of a dip in the middle of the spectrum. Thus, the proposed waveguide is found highly sensitive in case of horizontal deformation and even for 1° displacement could change the SCG bandwidth

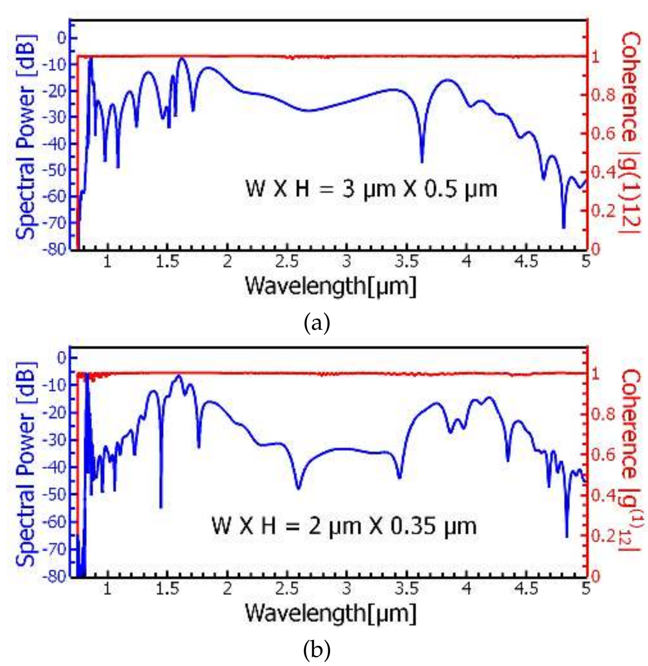

Fig. 9. First order complex degree of coherence $|g_{12}^{(1)}|$ and its corresponding SCG coverage for (a) the $LiNbO_3$ cladded waveguide with structural dimensions of W = 3 μm and H= 0.5 μm; (b) the MgF_2 cladded waveguide with dimensions of W = 2 μm and H= 0.35 μm, respectively.

at the waveguide output significantly.

Finally, the coherence of SCG spectra for the two most promising waveguides is tested with the aid of numerical simulations described in Dudley *et al.* [38]. The ensemble average of a number of different independent SCG spectra pairs $[E_1(\lambda_1), E_2(\lambda_2)]$ is generated with various random quantum noise seeds. The complex degree of 1st order coherence $|g_{12}^{(1)}|$ is used in this analysis which is defined in Gu *et al.* [39]. To analyze the coherence, an FWHM sech pulse of 50 fs is launched at 1.55 μm wavelength with an input peak power 50 W. Thirty independent SCG spectra pair ensemble average is calculated by adding a random noise of one photon per bin with the input pump pulse. The values of $|g_{12}^{(1)}|$ are depicted in Fig. 9 for two proposed structures over the entire spectral coverage region. In Fig. 9(a), the $|g_{12}^{(1)}|$ values are plotted with respect to wavelength for a $LiNbO_3$ cladded waveguide with structural dimensions of H= 0.5 μm, W = 3 μm. The similar results are obtained for the MgF_2 cladded waveguide with structural dimensions of W = 2 μm, H= 0.35 μm shown in Fig. 9(b). It is worth to be mentioned for both the plots that the value of $|g_{12}^{(1)}|$ is approximately unity i.e. $|g_{12}^{(1)}| \approx 1$ which implies the generated SCG spectra are highly coherent. The highly coherent SCG spectra generated by the proposed SRN waveguides can be promising for optical coherence tomography (OCT) applications [40].

CONCLUSION

In this numerical work, we propose CMOS compatible two 2 mm long planar waveguide models which can be made by the SRN material as a core and two different materials either $LiNbO_3$ or MgF_2 glass as top and bottom claddings for the broadband SCG coverage up to the MIR. The proposed waveguide structures are optimized by considering the pump source wavelength at 1.55 μm and the dimensional parameters of a waveguide i.e. H and W are varied to obtain an efficient SCG spectrum up to the MIR. Several structural formations of the waveguide by putting two different cladding materials as top and bottom are analyzed to obtain a wide anomalous GVD region dispersion curve with a smaller value of D at the pump wavelength. Among several GVD curves tailored during the linear analysis of waveguide geometries, four sets (each consists of three) of potential GVD curves are chosen for investigating the SCG in the MIR. Various waveguide models discussed during four sets of GVD curves tuning, two promising geometries, one is $LiNbO_3$ cladded and the other is MgF_2 cladded, are proposed for broadband SCG generation in the MIR. After rigorous analysis, it is found that the SCG coverage can be predicted from 0.8 to 4.6 μm with a low peak power of 50 W by the proposed models. This is, to the best of the authors' knowledge, the widest SCG coverage in the MIR by the SRN waveguide so far. Further increasing input power results flattened out the spectrum rather than expansion into the MIR. The effects of the occurrence of probable structural deformation of the proposed waveguides during fabrication are also discussed elaborately. It can be observed from simulation results that there is no significant change in the SCG coverage for occurring 10 degrees inside/outside (vertically) deformation during fabrication. However, it has been realized substantial spectral changes at the proposed waveguide output for upward/downward (horizontally) deformation during fabrication. Even one degree (1°) downward displacement can induce significant SCG bandwidth reduction (nearly 20 percent for the proposed model) at the waveguide output. Finally, coherence of the SCG spectra obtained from the proposed models is tested. Simulation result about coherence reveals highly coherent SCG at the output of either of the SRN waveguide proposed, which can be used in a variety of MIR region biological imaging and sensing applications.

REFERENCES

1. J. M. Dudley, G. Genty, and S. Coen, "Supercontinuum generation in photonic crystal fiber," Rev. Mod. Phys. **78**, 1135–1184 (2006).
2. J. M. Dudley and J. R. Taylor, "Ten years of nonlinear optics in photonic crystal fibre," Nat. Photonics **3**, 85 (2009).
3. C. Wei, X. Zhu, R. A. Norwood, F. Song, and N. Peyghambarian, "Numerical investigation on high power mid-infrared supercontinuum fiber lasers pumped at 3 µm," Opt. Express **21**, 29488–29504 (2013).
4. L. Liu, T. Cheng, K. Nagasaka, H. Tong, G. Qin, T. Suzuki, and Y. Ohishi, "Coherent mid-infrared supercontinuum generation in all-solid chalcogenide microstructured fibers with all-normal dispersion," Opt. letters **41**, 392–395 (2016).
5. J. Hu, C. R. Menyuk, L. B. Shaw, J. S. Sanghera, and I. D. Aggarwal, "Maximizing the bandwidth of supercontinuum generation in as2se3 chalcogenide fibers," Opt. Express **18**, 6722–6739 (2010).
6. J. S. Sanghera, L. B. Shaw, L. E. Busse, V. Q. Nguyena, P. C. Pureza, B. C. Cole, B. B. Harrison, I. D. Aggarwal, R. Mossadegh, F. Kung, D. Talley, D. Roselle, and R. Miklos, "Development and infrared applications of chalcogenide glass optical fibers," Fiber Integr. Opt. **19**, 251–274 (2000).
7. D. Duchesne, M. Peccianti, M. R. Lamont, M. Ferrera, L. Razzari, F. Légaré, R. Morandotti, S. Chu, B. E. Little, and D. J. Moss, "Supercontinuum generation in a high index doped silica glass spiral waveguide," Opt. Express **18**, 923–930 (2010).
8. V. R. Almeida, C. A. Barrios, R. R. Panepucci, and M. Lipson, "All-optical control of light on a silicon chip," Nature **431**, 1081 (2004).
9. R. Won and M. Paniccia, "Integrating silicon photonics," (2010).
10. M. Hochberg and T. Baehr-Jones, "Towards fabless silicon photonics," Nat. photonics **4**, 492 (2010).
11. T. Baehr-Jones, T. Pinguet, P. L. Guo-Qiang, S. Danziger, D. Prather, and M. Hochberg, "Myths and rumours of silicon photonics," Nat. Photonics **6**, 206 (2012).
12. B. Kuyken, F. Leo, S. Clemmen, U. Dave, R. Van Laer, T. Ideguchi, H. Zhao, X. Liu, J. Safioui, S. Coen *et al.*, "Nonlinear optical interactions in silicon waveguides," Nanophotonics **6**, 377–392 (2017).
13. M. Yang, L. Xu, J. Wang, H. Liu, X. Zhou, G. Li, and L. Zhang, "An octave-spanning optical parametric amplifier based on a low-dispersion silicon-rich nitride waveguide," IEEE J. Sel. Top. Quantum Electron. **24**, 1–7 (2018).
14. A. R. Johnson, A. S. Mayer, A. Klenner, K. Luke, E. S. Lamb, M. R. Lamont, C. Joshi, Y. Okawachi, F. W. Wise, M. Lipson *et al.*, "Octave-spanning coherent supercontinuum generation in a silicon nitride waveguide," Opt. letters **40**, 5117–5120 (2015).
15. D. K. Ng, Q. Wang, T. Wang, S.-K. Ng, Y.-T. Toh, K.-P. Lim, Y. Yang, and D. T. Tan, "Exploring high refractive index silicon-rich nitride films by low-temperature inductively coupled plasma chemical vapor deposition and applications for integrated waveguides," ACS applied materials & interfaces **7**, 21884–21889 (2015).
16. H. Zhao, B. Kuyken, S. Clemmen, F. Leo, A. Subramanian, A. Dhakal, P. Helin, S. Severi, E. Brainis, G. Roelkens *et al.*, "Visible-to-near-infrared octave spanning supercontinuum generation in a silicon nitride waveguide," Opt. letters **40**, 2177–2180 (2015).
17. R. Salem, Y. Okawachi, M. Yu, M. R. Lamont, K. Luke, P. Fendel, M. Lipson, and A. L. Gaeta, "Octave-spanning supercontinuum generation in a silicon nitride waveguide pumped by a femtosecond fiber laser at 1.9 μm," in *CLEO: Science and Innovations,* (Optical Society of America, 2015), pp. STu1I–7.
18. K. Luke, Y. Okawachi, M. R. Lamont, A. L. Gaeta, and M. Lipson, "Broadband mid-infrared frequency comb generation in a si 3 n 4 microresonator," Opt. letters **40**, 4823–4826 (2015).
19. J. P. Epping, T. Hellwig, M. Hoekman, R. Mateman, A. Leinse, R. G.

Heideman, A. van Rees, P. J. van der Slot, C. J. Lee, C. Fallnich *et al.*, "On-chip visible-to-infrared supercontinuum generation with more than 495 thz spectral bandwidth," Opt. express **23**, 19596–19604 (2015).

20. H. Ahmad, M. Karim, and B. Rahman, "Dispersion-engineered silicon nitride waveguides for mid-infrared supercontinuum generation covering the wavelength range 0.8–6.5 μm," Laser Phys. **29**, 025301 (2019).
21. T. Wang, D. K. Ng, S.-K. Ng, Y.-T. Toh, A. Chee, G. F. Chen, Q. Wang, and D. T. Tan, "Supercontinuum generation in bandgap engineered, back-end cmos compatible silicon rich nitride waveguides," Laser & Photonics Rev. **9**, 498–506 (2015).
22. X. Liu, M. Pu, B. Zhou, C. J. Krückel, A. Fülöp, M. Bache *et al.*, "Octave-spanning supercontinuum generation in a silicon-rich nitride waveguide," Opt. letters **41**, 2719–2722 (2016).
23. M. A. Porcel, F. Schepers, J. P. Epping, T. Hellwig, M. Hoekman, R. G. Heideman, P. J. van der Slot, C. J. Lee, R. Schmidt, R. Bratschitsch *et al.*, "Two-octave spanning supercontinuum generation in stoichiometric silicon nitride waveguides pumped at telecom wavelengths," Opt. express **25**, 1542–1554 (2017).
24. Y. Wang, S. Dai, X. Han, P. Zhang, Y. Liu, X. Wang, and S. Sun, "Broadband mid-infrared supercontinuum generation in novel As_2Se_3-As_2Se_2S step-index fibers," Opt. Commun. **410**, 410–415 (2018).
25. Y. Yu, B. Zhang, X. Gai, C. Zhai, S. Qi, W. Guo, Z. Yang, R. Wang, D.-Y. Choi, S. Madden *et al.*, "1.8-10 μm mid-infrared supercontinuum generated in a step-index chalcogenide fiber using low peak pump power," Opt. letters **40**, 1081–1084 (2015).
26. T. Cheng, K. Nagasaka, T. H. Tuan, X. Xue, M. Matsumoto, H. Tezuka, T. Suzuki, and Y. Ohishi, "Mid-infrared supercontinuum generation spanning 2.0 to 15.1 μm in a chalcogenide step-index fiber," Opt. letters **41**, 2117–2120 (2016).
27. D. E. Zelmon, D. L. Small, and D. Jundt, "Infrared corrected sellmeier coefficients for congruently grown lithium niobate and 5 mol.% magnesium oxide–doped lithium niobate," JOSA B **14**, 3319–3322 (1997).
28. M. J. Dodge, "Refractive properties of magnesium fluoride," Appl. Opt. **23**, 1980–1985 (1984).
29. M. Yoshida and P. N. Prasad, "Sol- gel-processed sio2/tio2/poly (vinylpyrrolidone) composite materials for optical waveguides," Chem. materials **8**, 235–241 (1996).
30. M. Karim, B. Rahman, and G. P. Agrawal, "Mid-infrared supercontinuum generation using dispersion-engineered $Ge_{11.5}As_{24}Se_{64.5}$ chalcogenide channel waveguide," Opt. express **23**, 6903–6914 (2015).
31. P. Ma, D.-Y. Choi, Y. Yu, X. Gai, Z. Yang, S. Debbarma, S. Madden, and B. Luther-Davies, "Low-loss chalcogenide waveguides for chemical sensing in the mid-infrared," Opt. express **21**, 29927–29937 (2013).
32. M. Karim, H. Ahmad, and B. A. Rahman, "All-normal-dispersion chalcogenide waveguides for ultraflat supercontinuum generation in the mid-infrared region," IEEE J. Quantum Electron. **53**, 1–6 (2017).
33. M. Butt, E. Kozlova, and S. Khonina, "Modeling of a straight channel and y-splitter waveguides by loading sio 2 planar waveguide with mgf 2," in *2017 Progress In Electromagnetics Research Symposium-Spring (PIERS),* (IEEE, 2017), pp. 2472–2477.
34. Y. Yu, X. Gai, T. Wang, P. Ma, R. Wang, Z. Yang, D.-Y. Choi, S. Madden, and B. Luther-Davies, "Mid-infrared supercontinuum generation in chalcogenides," Opt. Mater. Express **3**, 1075–1086 (2013).
35. M. R. Karim, B. Rahman, and G. P. Agrawal, "A broadband mid-infrared supercontinuum generation using $Ge_{11.5}As_{24}Se_{64.5}$ channel waveguide," in *Signal Processing in Photonic Communications,* (Optical Society of America, 2015), pp. JM3A–15.
36. A. Syahriar, R. R. Syms, and T. J. Tate, "Thermooptic interferometric switches fabricated by electron beam irradiation of silica-on-silicon," J. lightwave technology **16**, 841 (1998).
37. X. Gai, S. Madden, D.-Y. Choi, D. Bulla, and B. Luther-Davies, "Dispersion engineered $Ge_{11.5}As_{24}Se_{64.5}$ nanowires with a nonlinear parameter of 136 $W^{-1}m^{-1}$ at 1550 nm," Opt. express **18**, 18866–18874 (2010).
38. J. M. Dudley and S. Coen, "Numerical simulations and coherence properties of supercontinuum generation in photonic crystal and tapered optical fibers," IEEE J. selected topics quantum electronics **8**, 651–659 (2002).
39. X. Gu, M. Kimmel, A. P. Shreenath, R. Trebino, J. M. Dudley, S. Coen, and R. S. Windeler, "Experimental studies of the coherence of microstructure-fiber supercontinuum," Opt. Express **11**, 2697–2703 (2003).
40. A. Ghanbari, A. Kashaninia, A. Sadr, and H. Saghaei, "Supercontinuum generation for optical coherence tomography using magnesium fluoride photonic crystal fiber," Optik **140**, 545–554 (2017).

DISCLOSURES

The authors declare that there are no conflicts of interest related to this article.